Design, Fabrication, Testing, and Application of a Sub-Wavelength Microwave Lens

by

============

Submitted to the Department of Nuclear Science and Engineering
in partial fulfillment of the requirements for the degree of

Bachelor of Science in Nuclear Science and Engineering

at the

MASSACHUSETTS INSTITUTE OF TECHNOLOGY

June 2015

Author . . . .
Department of Nuclear Science and Engineering
May 8, 2015

Certified by. . . . .
========
====================
Thesis Supervisor

Accepted by . . . .
Michael P. Short
Assistant Professor, Nuclear Science and Engineering
Chair, NSE Committee for Undergraduate Students

Design, Fabrication, Testing, and Application of a Sub-Wavelength Microwave Lens

by

==============

Submitted to the Department of Nuclear Science and Engineering
on May 8, 2015, in partial fulfillment of the
requirements for the degree of
Bachelor of Science in Nuclear Science and Engineering

Abstract

Abstract here

Thesis Supervisor: ============
 Title: ====================

Acknowledgments

This is the acknowledgements section. You should replace this with your own acknowledgements.

Contents

List of Figures

List of Tables

1. Introduction

1.1 Motivation

The development of high power microwave (HPM) sources and related devices is a well-established and ever-growing field. A wide variety of disciplines depend on the use of HPM technology and consistently encourage further development. Common applications of HPM devices include radar, communication, industrial processing, and nuclear fusion experiments [1–5]. For many of these systems, the technology has been developed over decades of research and is now readily commercially available. In others, the demands placed on HPM devices encourage research using novel concepts to increase their performance and capabilities.

One example of these novel concepts is the development and use of metamaterial structures. Fundamentally, a metamaterial consists of a periodic structure whose period is smaller than the wavelength of light at the frequency of interest. Because the scale of variation is smaller than the wavelength, the metamaterial appears as a bulk material to the wave. The properties of the material the wave sees are determined by the metamaterial design. This allows them to exhibit properties not found in nature, such as a negative index of refraction. Substantial research has been done on metamaterials both in the microwave regime and in the optical regime. Major applications of metamaterials include cloaking, the creation of graded-index materials, improved solar power systems, and superlenses [6–11].

Graded-index materials and superlenses are particularly relevant to this work. In a graded-index material, the refractive index is not constant. Instead, it is varied over

the structure, allowing the material to alter the path of passing light in unique ways. Graded-index materials can be made from glass and other materials using a variety of manufacturing techniques, but they can also be created using metamaterial structures. The gradient of the index can be chosen by changing geometrical parameters of the metamaterial. This allows the index profile to be well-specified through the design process. Similarly, metamaterials can be used to create superlenses to focus light below the diffraction limit (see Section 2.2) [12–15]. Theoretically, they could even be used to create a perfect lens [16]. Conventional lenses only capture light which is propagating, but a perfect lens would also be able to capture evanescent waves. In systems like microscopes and telescopes, this would allow for the perfect resolution of an image. Thus, the optoelectronics community has a strong interest in creating the perfect lens and exploring superlensing structures [11].

In the microwave regime, the same principles apply. However, the use of metamaterials in high power systems is not always feasible. The small, often sub-millimeter structures can create areas of very high field which can cause break down easily. In these cases, photonic band gap (PBG) structures can be used [17]. These structures are created from rods arranged in a lattice. The structures are generally larger than a wavelength and are not susceptible to the same break down problems as metamaterials. Like metamaterials, geometrical parameters determine properties such as the effective refractive index of the structure. Variation in the geometry can be used to create a graded-index system, sometimes referred to as a graded-index photonic crystal. These structures are discussed in more detail in Section 2. By exploiting these principles, a lens created using a graded-index PBG structure could focus light below the diffraction limit.

1.1.1 Primary application

There are a number of possible applications for such a technology. A particularly interesting one is found in mining. The process of crushing and grinding rocks for mining (called comminution) is highly energy-intensive. It is estimated that some-

where between 3-5% of the world's electricity is used for comminution in various industries [18]. In the US, 1.5% of electricity generation is used in such material size reduction processes [19]. The current mechanical methods employed are highly inefficient and expensive, with efficiencies less than 1% [18, 19]. Given the amount and scale of mining operations worldwide, making this process more energy efficient would both reduce electricity consumption and save money.

One novel approach to improving comminution is using microwaves to rapidly heat certain minerals within the rocks before crushing or grinding. This creates thermal stresses large enough to cause microcracks along grain boundaries in the rocks. Studies have shown that microwave heating increases the grindability by up to 70% [20]. The microcracks decrease the structural integrity of the rock, allowing it to be mechanically crushed using much less energy. These effects have been well examined for many types of minerals [20–24]. It has been found that this effect is increased by using higher power densities, which in turn require less microwave energy input. Smaller rocks have been shown to require more energy to achieve the temperatures necessary for sufficient thermal stresses. A shorter pulse length is also more effective since it results in larger temperature gradients between the target minerals and the surrounding material [20].

Previous work in this area has primarily focused on the use of a microwave cavity to create standing waves [19]. The rock is placed in the microwave cavity for heating. This approach is problematic because it limits the size of rocks which can be heated to a few centimeters, which is not practical for an industrial-scale mining operation. Further, it reduces the speed at which the rocks can be processed. Microwave cavities are also typically made of materials which could easily be damaged from the harsh environment in mines [20]. Corrosion and other material damage over time would severely limit the lifetime of these devices, making them less desirable for use in industrial-scale operations. A new approach to this concept is needed in order to make microwave-assisted comminution possible at the industrial level.

The lens created for this project aims to address the problems typically found in

other microwave-assisted comminution designs. The lens can be used with a pulsed microwave source, which leads to short heating times and high thermal stresses. Unlike existing microwave-assisted comminution experiments, this lens does not require a cavity and could therefore be used on large rocks and could be more readily incorporated into a mining system. The lens can be built out of stronger and harder materials like steel instead of copper, reducing its susceptibility to wear and tear from the mining environment. Most importantly, the lens uses sub-wavelength focusing to create a higher power density in the focal spot, reducing required microwave energy input. This capability makes it an attractive technology for a variety of applications.

1.2   Project overview

This project includes the simulation, design, fabrication, and testing of a graded-index photonic band gap lens. The lens was designed to achieve sub-wavelength focusing at the a certain frequency, beating the traditional diffraction limit. A number of important factors had to be considered in the design process. First, the lens needed to be robust enough to operate at high power, avoiding problems with high fields and breakdown. For this reason, the PBG was designed using round rods. The sharp edges of square rods can create unwanted high field regions.

Additionally, the lens had to be designed for a frequency where the focal spot size could be accurately measured. At high frequencies, the focal spot size would become very small and therefore difficult to measure accurately. An accurate measurement of the focal spot size is needed to validate the focusing behavior of the lens and thus the lens was designed at a lower frequency. The larger spot size allows for a higher resolution of measurements in and around the focal spot, improving the accuracy of the results.

Further considerations were addressed in the actual fabrication of the lens. Several alterations were made to the lens structure over the course of the design process in order to make it easier to fabricate. Other alterations were made to ensure that the

lens would be appropriately rigid. Since the PBG behavior is highly geometrically-dependent, the fabrication tolerances on the rods had to be fairly small. Of the various fabrication methods examined, the one chosen was deemed the best at satisfying these and other practical constraints.

Testing of the lens created a number of demands. A probe had to be created which could measure the power inside the small vertical height of the lens. Very sensitive equipment had to be used in order to measure the power even with low coupling to the probe. To keep measurements consistent and accurate, a motorized scanner set up had to be used to change the probe's position. Each of these experimental solutions are discussed in more detail in Section 4.

2.   Background and Theory

This section will cover the relevant theoretical and technological information necessary to describe this project. It includes a brief discussion of refractive indices, dielectric constants, diffraction, and lenses. It also includes more information on the design and function of graded-index lenses and photonic band gap structures.

2.1   Refractive index and dielectric constant

The refractive index (or index of refraction) of a medium is a unitless expression of how light behaves when it propagates in the medium. It can be expressed as the ratio of the speed of light to the phase velocity of light in the medium, $n = \frac{c}{v}$. It can also be expressed as a function of relative permittivity ϵ_r and relative permeability μ_r, which are related to the electric and magnetic behavior of the wave as described in Maxwell's equations. The relative permittivity, often referred to as the dielectric constant, is simply the ratio of the electric permittivity of the medium to the vacuum permittivity, ϵ_0. Similarly, μ_r is the ratio of the magnetic permeability of the vacuum permeability μ_0.

The relation of these quantities to the index of refraction is $n = \sqrt{\epsilon_r \mu_r}$. Conventional, natural materials have positive refractive indices. In many metamaterial and PBG research efforts, the goal is to create materials with negative n.

2.2 Lenses and the diffraction limit

In the most general sense, a lens is simply a structure which is used to change the path of light. In the case of a convex lens, the light is focused to a focal spot. While lenses are most familiar in the optical regime where they're used in common devices like cameras and eyeglasses, they can be constructed in any frequency regime. At any frequency, there is a fundamental limit imposed on the focal spot size due to diffraction. Even with no other losses, a traditional lens cannot focus light to a spot smaller than this limit. This imposes restrictions on the possible resolution of devices like microscopes and telescopes. A general expression for the diffraction limit is

$$d = \frac{\lambda}{2n \sin \theta},$$ (2.1)

where d is the radius of the resolved spot, λ is the wavelength of the light, n is the refractive index of the medium, and θ is the angle of the incident spot [25, 26]. In the case of a lens with $n = 1$ and a 90deg incident angle (see Figure 2-1), this reduces to $d = \frac{\lambda}{2}$. This will be used as the diffraction limited spot radius for this work.
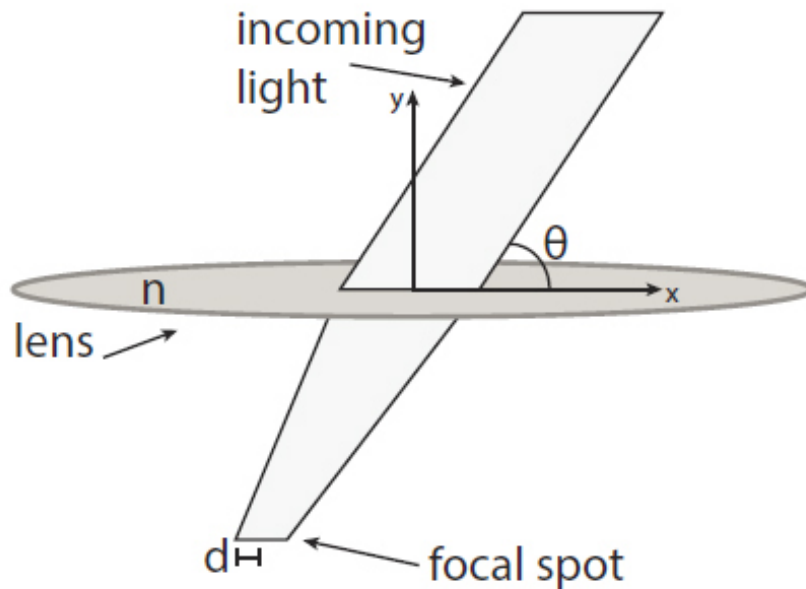

Figure 2-1: Schematic of light being focused with a convex lens. The light hits the lens of refractive index n at an angle θ. This creates a focal spot of radius d.

14

Beating the diffraction limit would allow better performance in a wide variety of devices. This would have to be done using a lens with a non-traditional index of refraction. Possible solutions include using graded-index materials or photonic band gap structures to create a lens with a negative index of refraction or graded-index profile. These topics are explored in the following sections.

2.3 Graded-index lenses

Graded-index devices are structures in which there is a gradient of the refractive index with position. A gradient can be created with traditional, positive refractive index materials. In these cases, the refractive index is usually largest at the center and gets smaller towards the edges of the device. Negative graded-index structures can also be created. In these devices, the modulus of the refractive index is smallest at the center axis of the device and increases outward. This allows the device to behave as a convex lens and focus a plane wave [27]. The graded negative index profile creates a number of interesting focusing effects [28–31]. It is possible to create a negative graded-index structure is through the use of metamaterials and PBG structures [12–15]. For the reasons discussed in Section 1.1, a PBG concepts were used as the basis for creating the graded-index structure for this project.

2.4 PBG structures

A photonic band gap structure consists of a periodic lattice of metal and/or dielectric rods. The dielectric constant changes with the use of different rod materials or air/vacuum gaps. This variation of the dielectric constant creates band gaps: any wave with a frequency within the band gap cannot propagate through the lattice. In the case of incident waves, the wave is reflected. PBG cavities can be created by removing rods to form a defect in the lattice. In these cases, the disallowed mode is confined in the defect region while other modes propagate out. Band gaps profiles

for cylindrical rods in triangular and square lattices have been calculated and are well-documented [17, 32, 33]. The size, arrangement, and material composition of the rods all affect the frequency and mode selectivity of the PBG, allowing the design of highly selective structures [17].

Figure 2-2 shows example square and triangular lattices as well as useful definitions of PBG geometrical parameters. Figure 2-3 shows the band gap maps for these lattices, calculated by [32]. These band gap maps show the areas of disallowed normalized frequency with respect to the ratio of the rod radius (a) to rod spacing (b). Within one lattice, a and b can be varied, thereby moving to a new location in the band gap map. By crossing into or out of a band gap, the refractive index changes. Thus by varying the size and/or spacing of rods, a GPC can be created as discussed in Section 2.3. These band gaps are calculated for the theoretical case of an infinite lattice. The band gaps for a finite lattice will be slightly different. However, it has been shown that PBG structures can achieve high performance with only a few rows of rods.
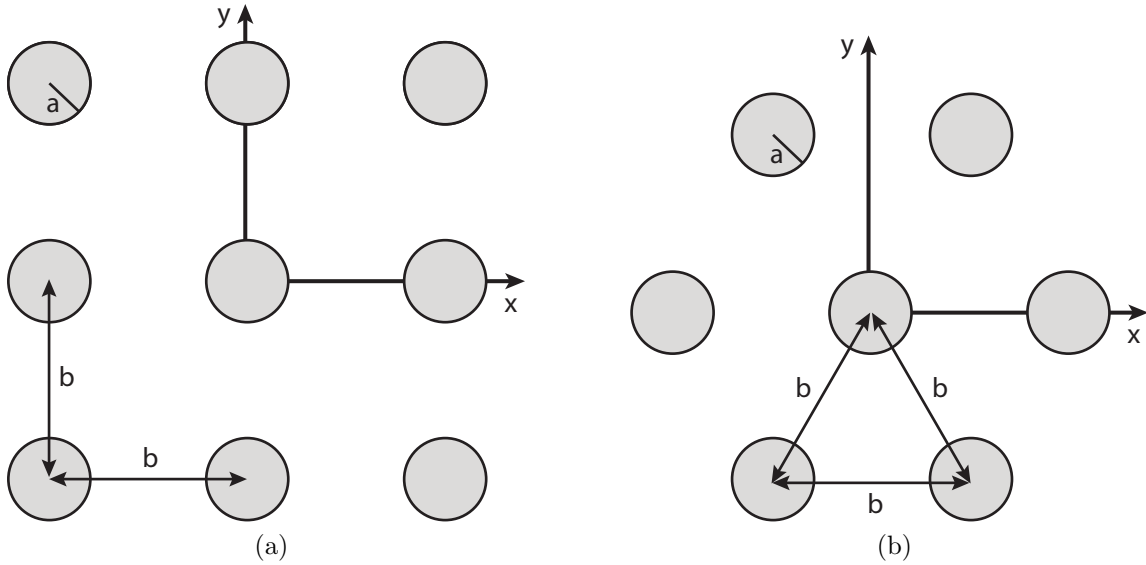

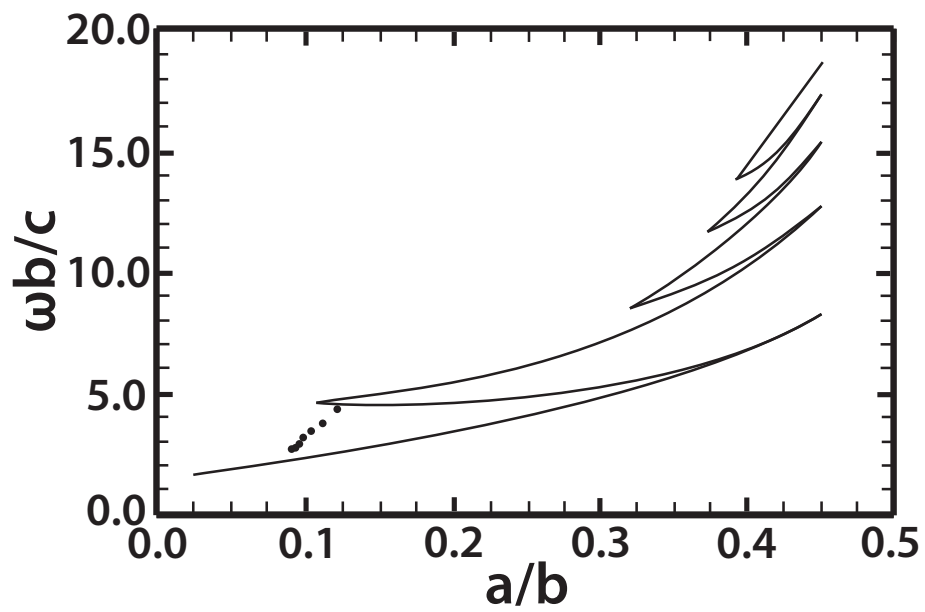Figure 2-2: Example square (a) and triangular (b) lattices, showing the meaning of rod spacing b and rod radius a.

16

Figure 2-3: Global band gaps for rods in a square lattice for transverse magnetic field modes, as a function of the rod radius to spacing (a/b) ratio. From left to right, the points correspond to rods 1-7 of the PBG lens (see Figure 3-1).

3. PBG lens design

The section details the process of designing the lens including challenges that were faced. It also contains an explanation of the final lens design and its predicted performance.

3.1 Simulations

The physics problems describing PBG performance are not easily analytically solvable. Thus in order to design and optimize this structure, it was necessary to use simulations. The simulations were performed using CST Microwave Studio, a commercially available software package for microwave device simulation [34]. The goal of the simulations was to determine the optimum number of rods as well as their size and spacing.

While PBG theory treats PBG lattices as infinite, in practice these devices generally only require a few rows of rods (a few periods) to achieve the desired performance. The optimum number was determined to be 7 rows with 14 rods in each column. Adding additional rows or columns beyond this point did not significantly improve the focusing capabilities of the lens. The lens has mirror symmetry across a plane through the fourth row as well as a plane between the 7th and 8th columns (see Figure 3-1).

Once this was determined, five parameters were adjusted: a, the spacing of the rods, b, the diameter of the rods, F_a, a scaling factor for the spacing, F_b, a scaling factor for the size, and m, a factor which determines the relationship between the
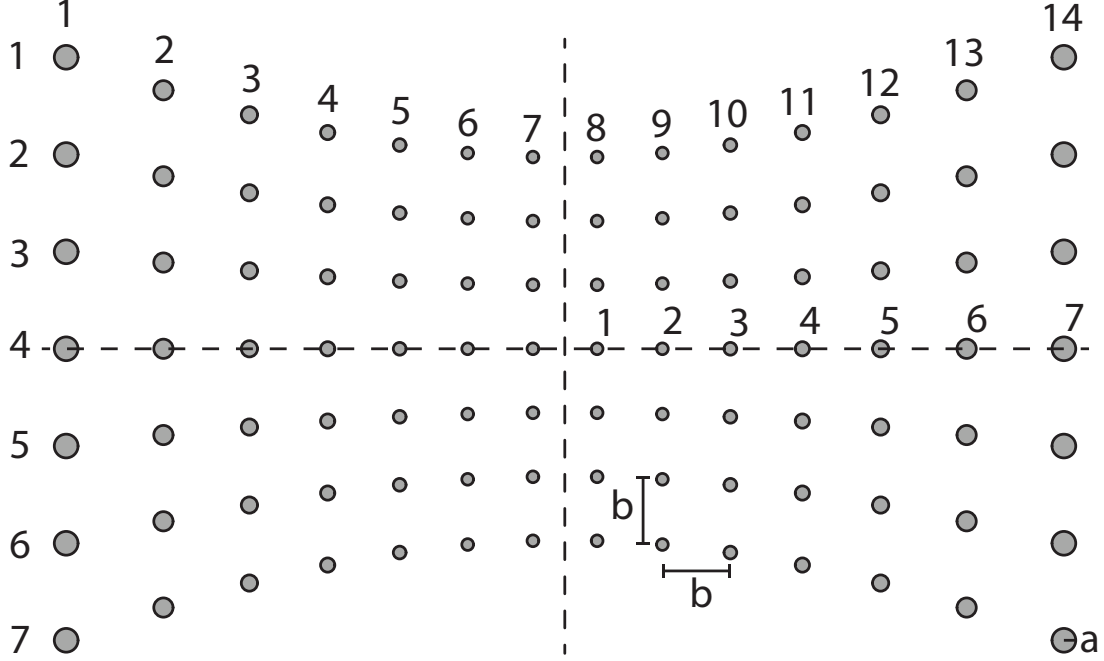
Figure 3-1: Scale schematic of the lens layout, showing the meaning of the rod spacing b and rod radius a. The dashed lines indicate the planes of symmetry. The row and column numbers are indicated above and alongside the lens. The rod index numbers n used in Equations 3.1&3.2 are shown along the center row.

spacing and diameter. The values of F_a and F_b are constant over the structure, but a and b change with each column. This was done to create a gradient in the refractive index over the structure. All the rods in a given column have the same a and b. The formulas describing the changes of a and b are

$$a_n = a_{(n-1)} F_a^{2(n-1)} \tag{3.1}$$

and

$$b_n = b_{(n-1)} F_b^{2(n-1)}, \tag{3.2}$$

where $n = 2, 3, ...7$ corresponds to the number of the rod counting from the center of the lens. The spacing of the first rod, a_1, is given by the formula

$$a_1 = m \frac{b_1}{5}. \tag{3.3}$$

19

The values of b_1, F_a, F_b, and m are then chosen, allowing all other values vary based on these factors.

In simulating the lens, the goal was to find the values of these parameters that cause a high peak value in the E field and a focal spot width smaller than the diffraction limit size. After numerous simulations, optimum values of these parameters were chosen. They are summarized in Table 3.1.

Parameter	Description	Optimum value
b_1	Spacing for rod 1	65 mm
F_a	Diameter scaling factor	1.0175
F_b	Spacing scaling factor	1.01
m	Diameter to spacing relation	0.9

Table 3.1: Optimum values of design parameters. These parameters together with Equations 3.1, 3.2, & 3.3 completely describe the geometry of the lens PBG structure.

Field profile for the chosen design is shown in Figure 3-2. The peak power is found at a frequency of 2.05 GHz, with smaller peaks at 1.95 and 2.2 GHz. The simulated focal spot width at the 1/e point is approximately 82.7 mm. The diffraction limited focal spot size can be calculated using Equation 2.1. At 2.05 GHz, $\lambda = 146.3$ mm. Thus, the predicted focal spot width is 0.565 times the diffraction limit. In all simulations, the height of the rods was 2 mm. When constructing a lens, a larger value had to be chosen to make fabrication feasible. The value was chosen to be 20 mm. New simulations were run at this value and the focal spot width was not affected.

3.2   Fabrication

The entire lens structure was direct machined in aluminum, which was chosen to minimize the cost and weight of the lens. The focusing behavior of the lens is not contingent on the material and losses at this frequency are small, so the lens could be built out of steel or a variety of other metals. In choosing a fabrication method, 3D printing was also considered. There are two main options: making the device purely
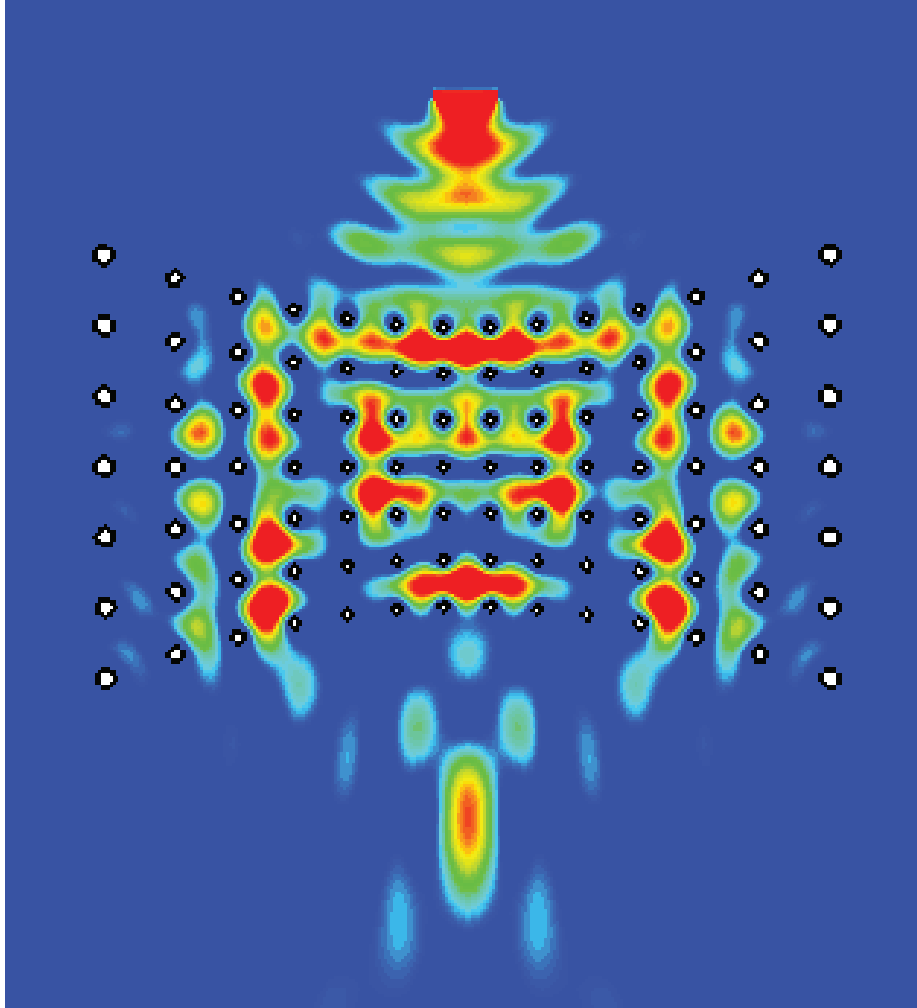
Figure 3-2: Electric field profile as simulated in CST Microwave Studio. The scale shows values from 1/e of the focal spot maximum to the focal spot maximum value. The white circles are the rods, and the wave is input from the top in this configuration.

from metal using Direct Metal Laser Sintering (DMLS), or 3D printing a plastic structure and adding a metal plating. Both of these options are readily available and could have been used to construct this device. However, it was determined that the 2D structure was simple enough to machine directly. For a more complicated design or one which has variations in 3 dimensions, 3D printing would be a superior choice.

The structure itself consists of two large, thin, metal plates which serve as the top and bottom of the lens. They lie in the same plane as the overhead view of the rod layout in Figure 3-1. The rods have tapped holes through their centers and are

attached directly to the plates on both sides to ensure good alignment. Originally, the rods were designed to sit in recessed pockets in the plates. However, this is more complicated to machine and would require thicker plates. It would require narrow fabrication tolerances on both the rods and the pockets to ensure the lens could be assembled correctly. Screwing the rods directly to the plates makes the lens simpler to machine by eliminating the need to create pockets of varying sizes. Additionally, the cost and weight of the lens can be reduced using this method. The metal plates are the largest physical parts of the lens and therefore make up most of the weight. By not requiring pockets, thinner plates can be used. Using this method does not negatively impact the device's performance, as the wave interacts only with a skin depth of the rod. A rod with a tapped hole and screws inside appears the same as a solid rod to the wave as long as the size of the rod is not comparable to the size of the rod. All of these factors contributed to the decision to attach the rods via screws

The plates had to be long enough to contain the field area shown in Figure 3-2. Because of this, there are large sections of the top plate which are not supported by any rods. To address this, a spacer post was added to each of the four corners. This provides support to the top plate to reduce stresses and eliminate bending. Two mounting brackets were designed to provide a place to attach equipment needed for testing. These were placed on the top and bottom plates on the input side of the lens. The input side (from where the input wave is launched) is on the end of the plate closer to the PBG lattice. The completed lens can be seen in Figure 3-3.
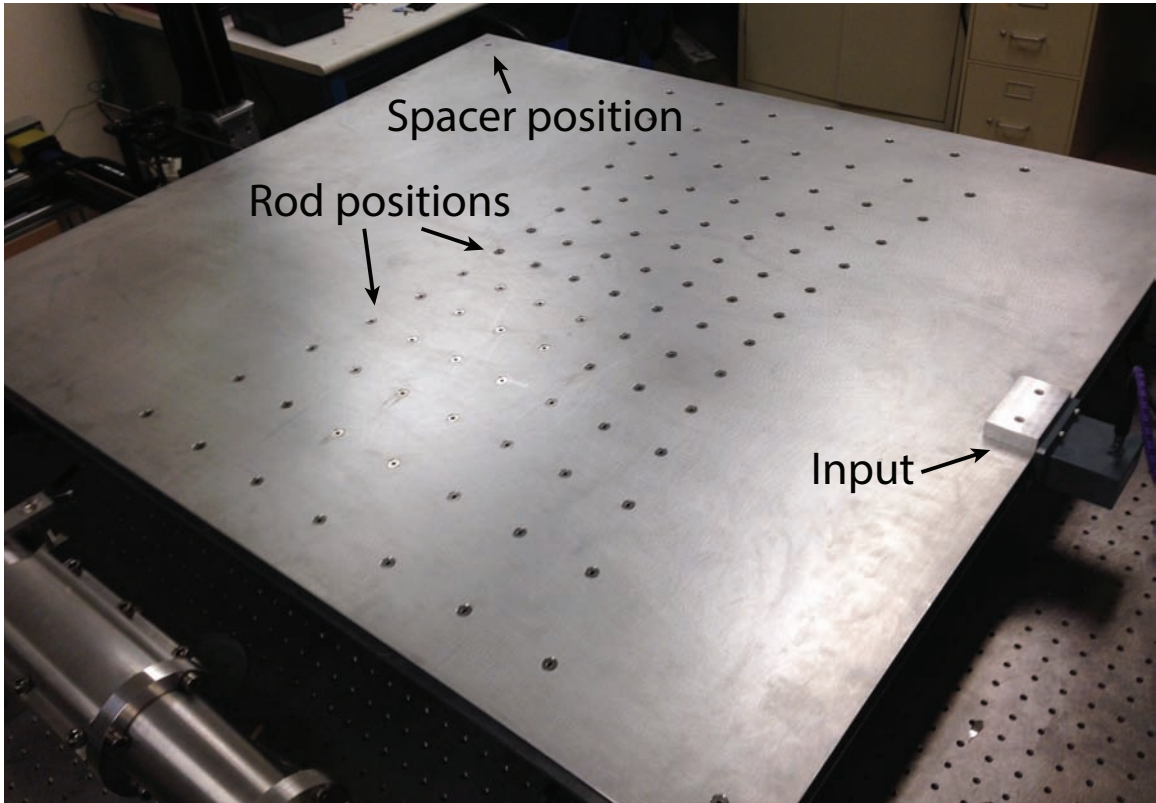
Figure 3-3: Overhead view of the completed lens. The screws used to attach the rods are visible, indicating the positions of the rods. The upper input mounting block is also shown. The position of one of the spacing posts can be seen at the top of the photo.

4. Experimental set-up

In order to determine the size of the focal spot, it was necessary to measure the power profile of the lens. To do this, the lens was connected to an Agilent E8363B vector network analyzer (VNA). Waves were launched into the lens using an S-band microwave head from the input side of the device, closer to the rods (see Figure 4-1). At the other end, a probe was inserted to measure the transmission (S_{12}). This measurement was repeated at varying positions in order to construct the field profile.
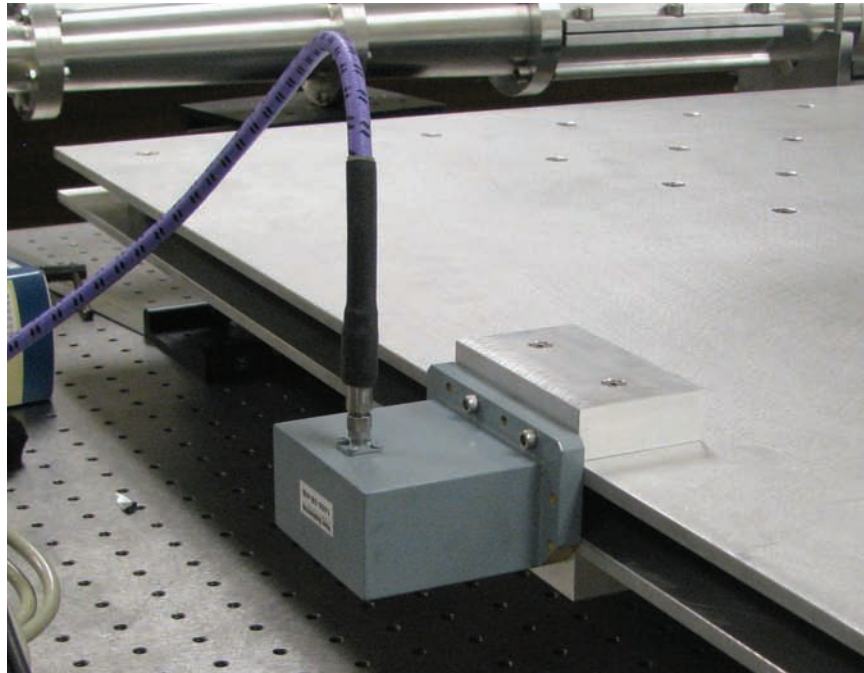

Figure 4-1: Input head of the VNA.

4.1 Probe

The simple probe constructed for this measurement consists of a small length of exposed wire, bent to be parallel with the electric field orientation. This wire is connected to an SMA cable which runs through a rigid pipe. The length of the interacting wire is 9 mm, a substantial portion of the 20 mm rod height. The probe is shown in Figure 4-2. The rigidity of the pipe ensured that the probe remained in good alignment with the electric field orientation as its position varied. In order to prevent reflections caused by the metal pipe, the probe is wrapped in ECCOSORB shielding.
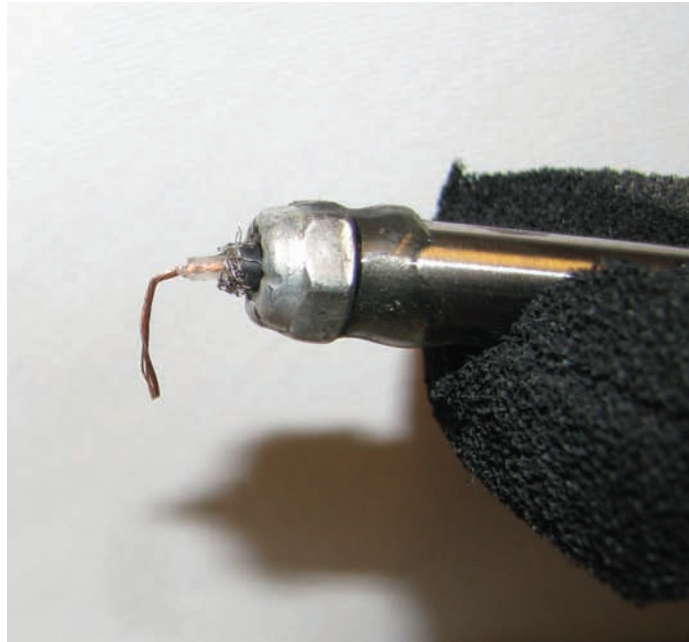

Figure 4-2: Tip of the probe, showing the interacting wire.

4.2 Scanner

Since the goal of this measurement was to examine the dependance of the electric field on probe position, it was necessary to obtain a high resolution of points over a large area of the lens. Manual movements of the probe are too inexact and cumbersome to

provide useful data. Instead, a motorized scanner set-up was used. The probe was fixed to the motorized stage which was then moved in steps over a specified area. The scanner recorded an S_{12} measurement at a specified frequency through the VNA. This allowed for easy adjustment of the measured frequency, step size, and scan area. The scanner set-up can be seen in Figure 4-3. Scans were taken at a variety of frequencies surrounding the design frequency of 2.05 GHz. This was done in order to demonstrate the minimization of the focal spot width near the desired frequency.
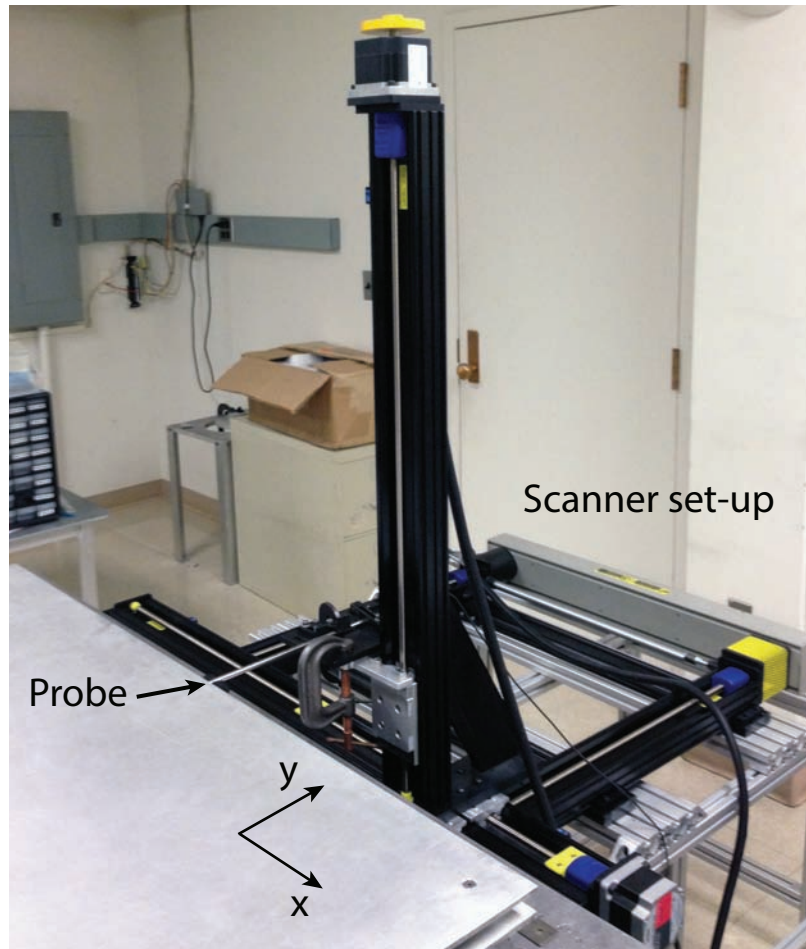

Figure 4-3: Scanner set-up used for data collection. The end of the probe pipe can be seen outside the lens. The scanner has 3 planes of possible movement, but only two were used for these measurements. The scan directions are indicated by the x-y axes.

5. Experimental results

Scans of the power profile in the lens were taken to determine the focal spot size at various frequencies. Points were chosen surrounding the design frequency of 2.05 as well as farther away in order to show the difference in focusing performance with frequency. At each frequency, the spot size was calculated and compared to the diffraction limit. The ratio of the measured size to the diffraction limited size was calculated to determine whether the lens beat the diffraction limit. There are two possible ways to define the spot size, each with their own corresponding limit. The first is measuring the width from where the power is $1/e^2$ of the maximum value on either side of the maximum. This size corresponds to the diffraction limit discussed in Section 2.2, which is one wavelength. Another is to measure the full width at half maximum (FWHM) of the spot. In this case, the corresponding traditional diffraction limit is one half of a wavelength. The results of these calculations are shown in Figure 5-1.

Overall, the lens was able to beat the diffraction limit at all measured points. The spot is smallest in the area around the design frequency, but is still measurably smaller than the diffraction limit at other frequencies. For the FWHM size, there is a clear consistent trend: the lens performs better closer to its optimum point. The $1/e^2$ size is more variable. By both metrics, the best performance was found at 2.068 GHz. This is slightly shifted from the simulated design frequency of 2.05 GHz, possibly due to small errors in fabrication that altered the sizes of some rods. The measured power profile at this frequency is shown in Figure 5-2. At this frequency, the $1/e^2$ size was measured to be approximately 92.5 mm, and the FWHM was approximately 50 mm.
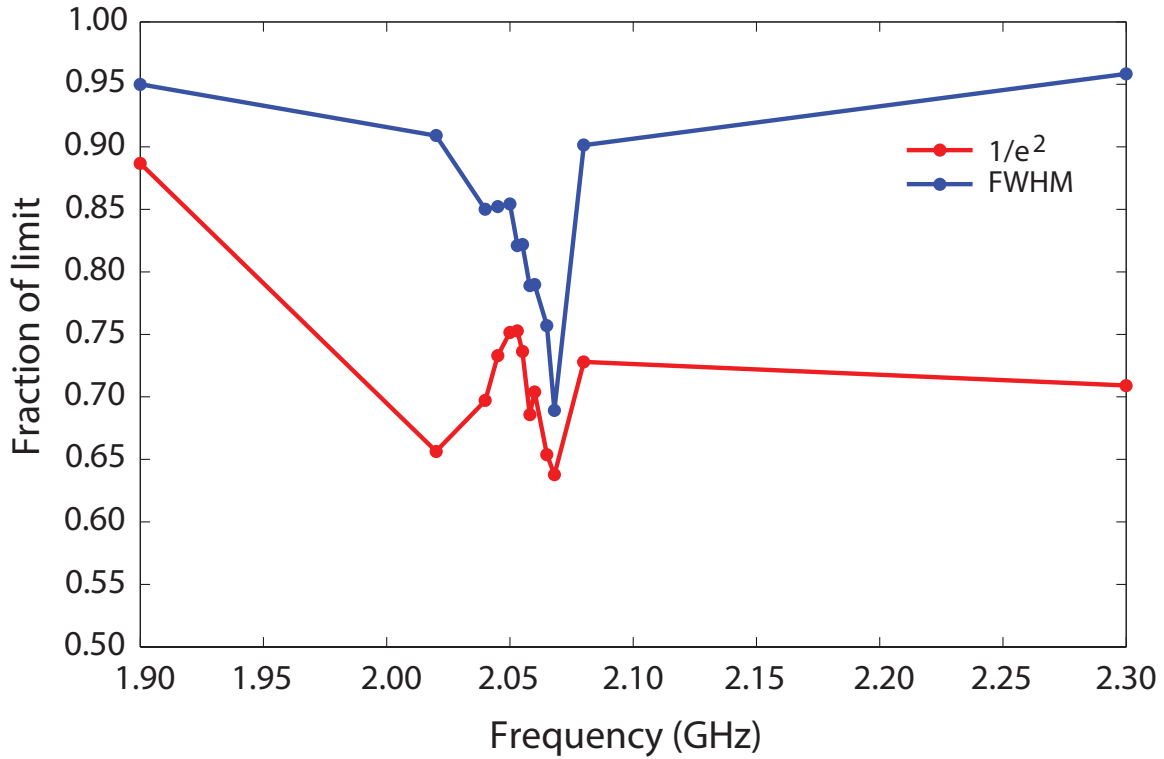
Figure 5-1: Plot of the spot size at each point normalized to the diffraction limit size at that point. Since all values are below 1, they beat the diffraction limit.

These values correspond to 0.64 and 0.68 times the diffraction limit, respectively. This is greater than the predicted value of 0.565, but still substantially below the limit.

Interestingly, the focal spot is shorter in length than was predicted by simulation. The highest power is concentrated into a nearly circular region, rather than the oblong region predicted. It is possible that this is the result of some fabrication error, but further studies are needed to conclude the source of this difference.
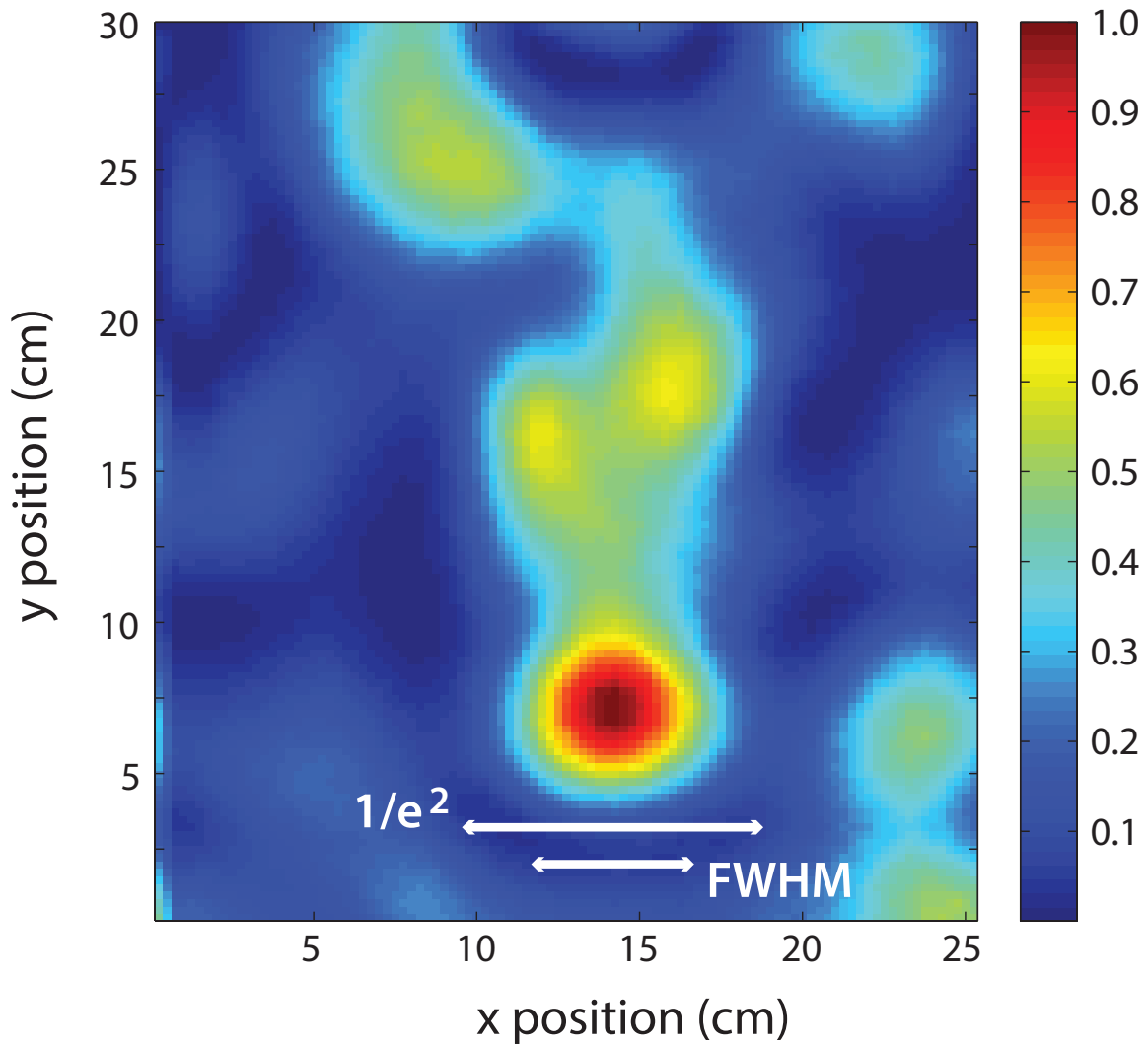
Figure 5-2: Measured power profile at 2.068 GHz, normalized to the maximum frequency. The focal spot has substantially higher power than the surrounding area. The widths of the $1/e^2$ and FWHM sizes are shown to scale beneath the spot.

6. Conclusions

A graded-index lens was designed using a photonic band gap structure with the intention of beating the traditional diffraction limit. An extensive simulation and optimization process was used to design the lens, which was then fabricated and tested.

Measurements have shown the lens can focus to spot sizes smaller than the diffraction limit at a range of frequencies around the design point. The optimum performance point of the lens was found to be 2.068 GHz, a shift from the simulated value of 2.05 GHz. At this point, the spot size is 0.64 times the diffraction limit. This is close to the value predicted by simulations, and a substantial improvement over the diffraction limit. This lens is a successful demonstration of the use of PBG structures and graded-index principles to achieve sub-wavelength focusing. Further, it shows fairly good performance over a range of frequencies, which could be exploited in certain applications.

This lens is a 2D PBG lattice. There is the potential to move to a 3D structure, which essentially would consist of layers of lattices in different orientations. This would allow easier access to the focal spot, making the lens easier to incorporate into different systems. Due to the size of the structure at this frequency, moving to a higher frequency would be advisable if a 3D lens were constructed.

Bibliography

[1] N. Kumar, U. Singh, T.P. Singh, and A.K. Sinha. A review on the applications of high power, high frequency microwave source: Gyrotron. *Journal of Fusion Energy*, 30(4):257–276, 2011.

[2] C.R. Smith, C.M. Armstrong, and J. Duthie. The microwave power module: a versatile rf building block for high-power transmitters. *Proceedings of the IEEE*, 87(5):717–737, May 1999.

[3] N. Srirattana, A. Raghavan, D. Heo, P.E. Allen, and J. Laskar. Analysis and design of a high-efficiency multistage doherty power amplifier for wireless communications. *Microwave Theory and Techniques, IEEE Transactions on*, 53(3):852–860, March 2005.

[4] C. Leonelli and T.J. Mason. Microwave and ultrasonic processing: Now a realistic option for industry. *Chemical Engineering and Processing: Process Intensification*, 49(9):885 – 900, 2010.

[5] M. Thumm. High power gyro-devices for plasma heating and other applications. *International Journal of Infrared and Millimeter Waves*, 26(4):483–503, 2005.

[6] D. Schurig, J.J. Mock, B.J. Justice, S.A. Cummer, J.B. Pendry, A.F. Starr, and D.R. Smith. Metamaterial electromagnetic cloak at microwave frequencies. *Science*, 314(5801):977–980, 2006.

[7] P. Alitalo and S. Tretyakov. Electromagnetic cloaking with metamaterials. *Materials Today*, 12(3):22 – 29, 2009.

[8] B. Vasic, G. Isic, R. Gajic, and K. Hingerl. Controlling electromagnetic fields with graded photonic crystals in metamaterial regime. *Opt. Express*, 18(19):20321–20333, Sep 2010.

[9] C. Wu, B. Neuner III, J. John, A. Milder, B. Zollars, S. Savoy, and G. Shvets. Metamaterial-based integrated plasmonic absorber/emitter for solar thermo-photovoltaic systems. *Journal of Optics*, 14(2):024005, 2012.

[10] Y. Wang, T. Sun, T. Paudel, Y. Zhang, Z. Ren, and K. Kempa. Metamaterial-plasmonic absorber structure for high efficiency amorphous silicon solar cells. *Nano Letters*, 12(1):440–445, 2012.

[11] X. Zhang and Z. Liu. Superlenses to overcome the diffraction limit. *Nature Materials*, 7:435–441, 2008.

[12] A. Grbic and G.V. Eleftheriades. Overcoming the diffraction limit with a planar left-handed transmission-line lens. *Physical Review Letters*, 92:117403, Mar 2004.

[13] K. Aydin, I. Bulu, and E. Ozbay. Subwavelength resolution with a negative-index metamaterial superlens. *Applied Physics Letters*, 90(25):254102, 2007.

[14] T. Driscoll, D.N. Basov, A.F. Starr, P.M. Rye, S. Nemat-Nasser, D. Schurig, and D.R. Smith. Free-space microwave focusing by a negative-index gradient lens. *Applied Physics Letters*, 88(8):081101, 2006.

[15] G.X. Li, H.L. Tam, F.Y. Wang, and K.W. Cheah. Superlens from complementary anisotropic metamaterials. *Journal of Applied Physics*, 102(11):116101, 2007.

[16] J.B. Pendry. Negative refraction makes a perfect lens. *Physical Review Letters*, 85:3966–3969, Oct 2000.

[17] M.A. Shapiro, C. Chen, J.R. Sirigiri, E.I. Smirnova, and R.J. Temkin. Photonic bandgap structures for high power microwave applications. In *Microwave Symposium Digest, 2004 IEEE MTT-S International*, volume 2, pages 1005–1008 Vol.2, June 2004.

[18] M. Rhodes. *Introduction to Particle Technology*. John Wiley and Sons Ltd., Chichester, England, 2nd edition, 2008.

[19] D.N. Whittles, S.W. Kingman, and D.J. Reddish. Application of numerical modelling for prediction of the influence of power density on microwave-assisted breakage. *International Journal of Mineral Processing*, 68:71–91, 2003.

[20] S.W. Kingman. Recent developments in microwave processing of minerals. *International Materials Reviews*, 51(1):1–12, 2006.

[21] T.T. Chen, J.E. Dutrizac, K.E. Haque, W. Wyslouzil, and S. Kashyap. The relative transparency of minerals to microwave radiation. *Canadian Metallurgy Quarterly*, 23(1):349–351, 1984.

[22] S. Kingman. *The effect of microwave radiation on the comminution and beneficiation of minerals and ores*. PhD thesis, University of Birmingham, 1998.

[23] S.W. Kingman, K. Jackson, S.M. Bradshaw, N.A. Rowson, and R. Greenwood. An investigation into the influence of microwave treatment on mineral ore comminution. *Powder Technology*, 146:176–184, 2004.

[24] S.W. Kingman, W. Vorster, and N.A. Rowson. The influence of mineralogy on microwave assisted grinding. *Minerals Engineering*, 13(3):313–3227, 2000.

[25] S.G. Lipson and H. Lipson. *Optical Physics*. Cambridge University Press, 1969.

[26] S. Solimeno, B. Crosignani, and P. DiPorto. *Guiding, Diffraction, and Confinement of Optical Radiation*. Academic Press, Inc., 1986.

[27] Q. Wu, J.M. Gibbons, and W. Park. Graded negative index lens by photonic crystals. *Optics Express*, 16(21):16941–16949, 2008.

[28] H. Kurt, E. Colak, O. Cakmak, H. Caglayan, and E. Ozbay. The focusing effect of graded index photonic crystals. *Applied Physics Letters*, 93(17):171108, 2008.

[29] F. Gaufillet and E. Akmansoy. Graded photonic crystals for graded index lens. *Optics Communications*, 285(1011):2638 – 2641, 2012.

[30] C. Tan, T. Niemi, C. Peng, and M. Pessa. Focusing effect of a graded index photonic crystal lens. *Optics Communications*, 284(12):3140 – 3143, 2011.

[31] M. Turduev, I.H. Giden, and H. Kurt. Design of flat lens-like graded index medium by photonic crystals: Exploring both low and high frequency regimes. *Optics Communications*, 339(0):22 – 33, 2015.

[32] E.I. Smirnova, C. Chen, M.A. Shapiro, J.R. Sirigiri, and R.J. Temkin. Simulation of photonic band gaps in metal rod lattices for microwave applications. *Journal of Applied Physics*, 91(3):960–968, 2002.

[33] E.I. Smirnova. Photonic band gap structures for accelerator applications. *AIP Conference Proceedings*, 737(1):309–319, 2004.

[34] Computer Simulation Technology. Cst microwave studio. `http://www.cst.com/`. Accessed: 2015-04-27.

22.THT Undergraduate Thesis Tutorial
Fall 2015